Graphene Oxide Attenuates Toxicity of Amyloid-β Aggregates in Yeast by Promoting Disassembly and Boosting Cellular Stress Response

Optimizing Interface Conductivity in Electronics

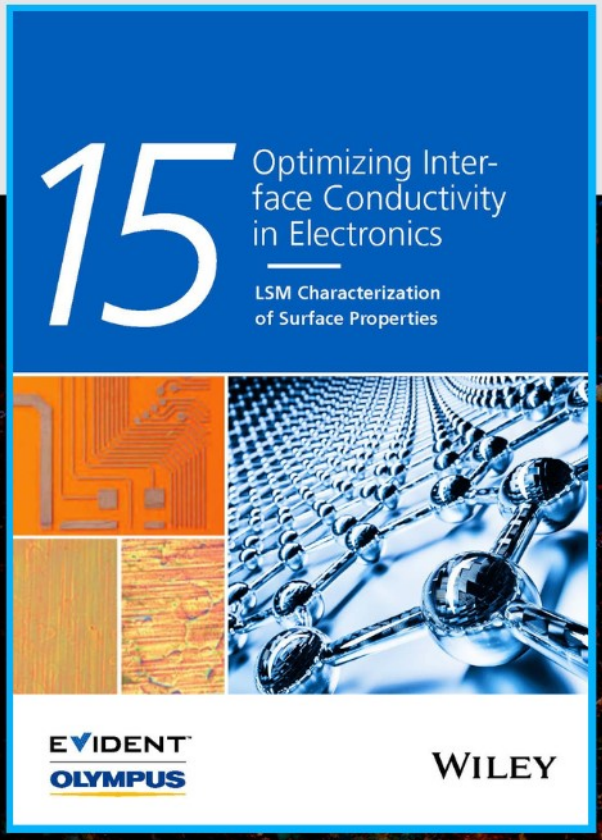

The latest eBook from Advanced Optical Metrology. Download for free.

Surface roughness is a key parameter for judging the performance of a given material's surface quality for its electronic application. A powerful tool to measure surface roughness is 3D laser scanning confocal microscopy (LSM), which will allow you to assess roughness and compare production and finishing methods, and improve these methods based on mathematical models.

Focus on creating high-conductivity electronic devices with minimal power loss using laser scanning microscopy is an effective tool to discern a variety of roughness parameters.

EVIDENT
OLYMPUS

WILEY

ADVANCED FUNCTIONAL MATERIALS
www.afm-journal.de

Graphene Oxide Attenuates Toxicity of Amyloid-β Aggregates in Yeast by Promoting Disassembly and Boosting Cellular Stress Response

Xin Chen, Santosh Pandit, Lei Shi, Vaishnavi Ravikumar, Julie Bonne Køhler, Ema Svetlicic, Zhejian Cao, Abhroop Garg, Dina Petranovic, and Ivan Mijakovic**

Alzheimer's disease (AD) is the most prevalent neurodegenerative disease, with the aggregation of misfolded amyloid-β (Aβ) peptides in the brain being one of its histopathological hallmarks. Recently, graphene oxide (GO) nanoflakes have attracted significant attention in biomedical areas due to their capacity of suppressing Aβ aggregation in vitro. The mechanism of this beneficial effect has not been fully understood in vivo. Herein, the impact of GO on intracellular Aβ42 aggregates and cytotoxicity is investigated using yeast *Saccharomyces cerevisiae* as the model organism. This study finds that GO nanoflakes can effectively penetrate yeast cells and reduce Aβ42 toxicity. Combination of proteomics data and follow-up experiments show that GO treatment alters cellular metabolism to increases cellular resistance to misfolded protein stress and oxidative stress, and reduces amounts of intracellular Aβ42 oligomers. Additionally, GO treatment also reduces HTT103QP toxicity in the Huntington's disease (HD) yeast model. The findings offer insights for rationally designing GO nanoflakes-based therapies for attenuating cytotoxicity of Aβ42, and potentially of other misfolded proteins involved in neurodegenerative pathology.

1. Introduction

Accumulation and aggregation of misfolded amyloid-β (Aβ) peptides in the brain is thought to be an early driver of Alzheimer's disease (AD), which is an incurable brain disease leading to dementia and death.[1] It is estimated that approximately 44 million people worldwide are living with AD or a related form of dementia. Besides the suffering of the patients and their families, the estimated global cost of AD and dementia is around $605 billion, which is the equivalent of 1% of the entire world's gross domestic product. The formation of Aβ aggregates is believed to be a net result of imbalance between Aβ production and clearance.[2] Aβ peptides abnormally aggregate from soluble monomers into oligomers, protofibrils, and insoluble fibrils. Reduced clearance of Aβ could also result in accumulation of its aggregates. This in turn triggers a cascade of pathogenic processes including neuroinflammation, neurofibrillary tau-tangle formation, and progressive synaptic dysfunction.[3] Despite many efforts committed to the search for anti-amyloid agents, no breakthroughs have been made with potential treatments in clinical trials so far.[4]

Graphene and its hydrophilic derivative graphene oxide (GO) are 2D sp^2-hybridized carbon nanomaterials that have been largely explored in biomedical applications including cancer therapies, drug delivery and biosensing.[5] These materials have some unique properties, such as high carrier mobility, unparalleled thermal conductivity, and excellent biocompatibility. Several in vitro studies demonstrated that GO sheets can inhibit the Aβ fibrillization process through adsorption of amyloid monomers,[6] and cutting mature amyloid fibrils, which promotes their clearance.[7] A computational simulation also suggested that the Aβ fibrils display strong interactions with graphene, which effectively inhibits the self-association and aggregation of Aβ.[8] Recently, studies on a mouse AD model showed that GO nanoflakes could ameliorate cognitive impairment through clearing the deposition of Aβ.[9] However, the mechanism of this beneficial effect of GO nanoflakes has not been completely illuminated in vivo.

X. Chen, S. Pandit, L. Shi, Z. Cao, D. Petranovic, I. Mijakovic
Division of Systems and Synthetic Biology
Department of Life Sciences
Chalmers University of Technology
Gothenburg 41296, Sweden
E-mail: cxin@chalmers.se; ivan.mijakovic@chalmers.se
X. Chen, D. Petranovic
Novo Nordisk Foundation Center for Biosustainability
Chalmers University of Technology
Gothenburg 41296, Sweden
V. Ravikumar, J. B. Køhler, E. Svetlicic, A. Garg, D. Petranovic, I. Mijakovic
Novo Nordisk Foundation Center for Biosustainability
Technical University of Denmark
Lyngby 2800, Denmark

The ORCID identification number(s) for the author(s) of this article can be found under https://doi.org/10.1002/adfm.202304053

DOI: 10.1002/adfm.202304053

With the ease of genetic manipulation, as well as available databases and computational models, yeast is a robust in vivo tool to study proteins involved in human disease and related intracellular processes.[10] Due to a strong evolutionary conservation of the cellular protein quality control systems between yeast and humans, the yeast *Saccharomyces cerevisiae* is particularly useful for studying protein aggregation and proteostasis, which are relevant features for AD, Huntington's disease (HD), Parkinson's disease (PD) and other incurable protein misfolding diseases.[11] Aβ is one of the main peptides relevant for AD pathologies. Aβ42 and Aβ40 are two major forms of Aβ, with 42 and 40 amino acid residues, respectively. With its two extra amino acids, Aβ42 is the more hydrophobic of the two, and more prone to forming aggregates. This form of Aβ is enriched in patients diagnosed with AD.[12] In previous studies, we have established a yeast model by constitutively expressing Aβ42 with the ER targeting signal fused to its N terminus.[13] After the signal sequence is cleaved, Aβ42 transits through the secretory pathway to the plasma membrane and is internalized again through endocytosis.[14] Increased Aβ42 production and aggregation caused a strong phenotype in this yeast Aβ model, comprising cytotoxicity, faster ageing, ER stress, mitochondrial dysfunction, and elevated reactive oxygen species (ROS) production.[13,15] This complex phenotype is similar to the phenotypes of human neurons affected with Aβ.[16]

In this study, we applied our yeast Aβ42 model[13,15] to study the internalization and intracellular mechanisms of action of GO nanoflakes. Using this model, we found that GO nanoflakes can effectively penetrate yeast cells, improve cell viability, and reduce key features of the Aβ42-associated phenotype. Namely, GO-treated cells exhibited an increased capacity to cope with misfolded protein stress and oxidative stress. In addition to boosting cellular stress response, GO nanoflakes specifically depleted intracellular high molecular weight of Aβ42 oligomers, which are considered to be the toxic forms. While GO nanoflakes were not able to protect other classes of proteins from misfolding in vitro, they did reduce HTT103QP toxicity in the yeast HD model, presumably by a similar mechanism. This suggests a potentially broader significance of the reported phenomenon for incurable misfolding-related diseases.

2. Results and Discussion

2.1. GO Nanoflakes Coat Aβ42-Expressing Yeast Cells and get Internalized, but They Do Not Compromise Physical Integrity of Yeast

Commercially available GO nanoflakes were sonicated to produce flakes with an average size of 90 nm, as determined by dynamic light scattering (DLS). The properties of the GO nanoflakes were characterized with scanning electron microscopy (SEM), transmission electron microscopy (TEM), and Raman spectroscopy (Figure S1, Supporting Information). In SEM and TEM images, the GO nanoflakes demonstrated a wrinkled morphology and their dimensions were on average within the size range of 70–110 nm in length/width, which is consistent with the average size of 90 nm determined by the DLS measurement. The Raman spectrum of the GO nanoflakes showed the I(D)/I(G) ratio of 1.13, suggesting that the sp^3-hybridized domain is larger than the sp^2-hybridized domain in the obtained GO nanoflakes.

The Aβ42 yeast strain was cultivated to early exponential phase (OD_{600} ≈1), and then mixed with the prepared GO flakes with concentration of 50 and 100 μg mL^{-1}, respectively. The growth experiment was resumed in the same conditions, and after 48 h of exposure to GO nanoflakes, SEM was used to examine the cell morphology (Figure S2, Supporting Information). The cell surface was found to be covered with GO flakes, indicating the physical interaction. All the examined GO nanoflakes-treated cells retained their morphological integrity, indicating that the interaction with GO nanoflakes was not harmful. TEM was used to investigate the internalization of GO nanoflakes by Aβ42 cells after 48 h of exposure. GO nanoflakes were detected inside cells (**Figure 1**), with no obvious concentration dependence. The majority of GO nanoflakes were found within vacuoles. The vacuoles provide an acidic environment, containing conserved proteases and other hydrolytic enzymes, which are responsible for the degradation of damaged organelles and proteins aggregates, including Aβ42 aggregates.[17]

2.2. GO Nanoflakes Reduce Aβ42 Cytotoxicity

To test whether the GO nanoflakes protect cells against deleterious effects of expressing Aβ42, we evaluated cellular viability in the presence of either 50 or 100 μg mL^{-1} of GO nanoflakes in the culture medium following a chronological life span (CLS). The CLS is defined as the survival time of nondividing cells and it is proposed as an aging model for post-mitotic tissues in mammals, such as neurons.[18] The Aβ42 strain was cultivated to early exponential phase (OD_{600} ≈1) and treated with GO nanoflakes. Cellular viability was measured by propidium iodide (PI) staining every day. Live and dead cells were separated and counted by flow cytometry. Treatments with both concentrations of GO nanoflakes significantly increased the viability of the Aβ42 strain throughout the CLS ($p < 0.05$, **Figure 2**a). We further examined whether the size of GO nanoflakes could have an impact on their effect on the Aβ42 strain. In addition to our standard nanoflakes (mean diameter of 90 nm), we prepared two batches of larger flakes, with mean diameters of 220 and 250 nm. Larger flakes had a slightly stronger beneficial effect on cell survival during the CLS, but the difference was not statistically significant ($p > 0.05$, Figure S3a, Supporting Information). However, the size of GO flakes affected their dispersibility in the culture medium. While the 90 nm flakes remained uniformly dispersed during the 7-day CLS experiment, larger flakes aggregated into insoluble clumps (Figure S3b, Supporting Information). Aggregation is most likely to limit applicability of larger nanoflakes, hence we continued our investigation with the 90 nm GO nanoflakes.

2.3. GO Nanoflakes Causes a Global Proteome Response in Aβ42-Expressing Yeast Cells

AD is a complex disease, involving an interplay of many cellular networks, and the involvement of Aβ42 in the disease is presumably equally complex.[19] In order to clarify the mechanism by which GO nanoflakes help to reduce Aβ42 cytotoxicity, we

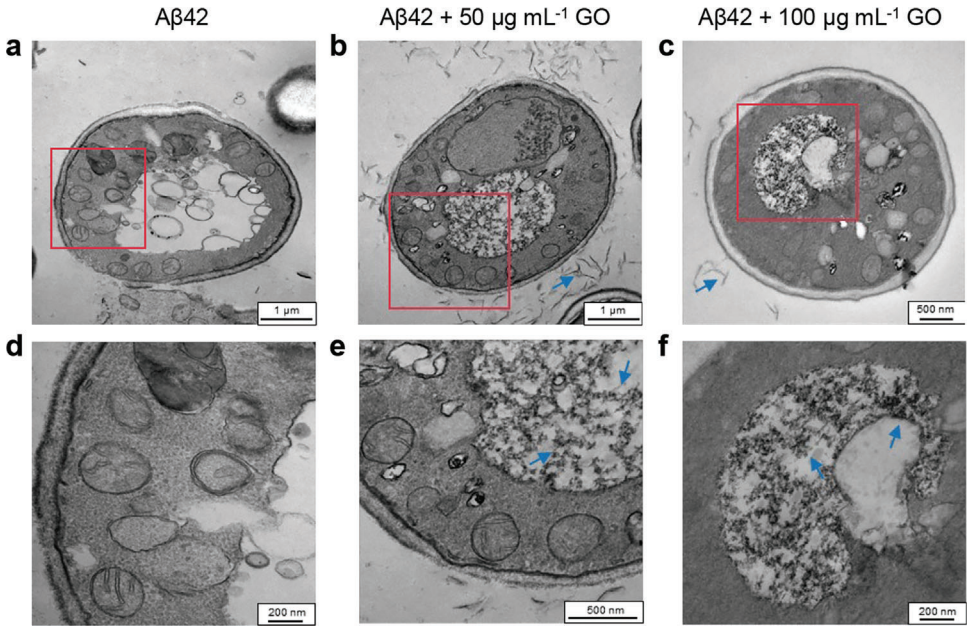

Figure 1. Internalization of GO nanoflakes into Aβ42-expressing cells. TEM images of a) Aβ42 strain, b) Aβ42 strain treated with 50 μg mL^{-1} of GO nanoflakes, and c) Aβ42 strain treated with 100 μg mL^{-1} of GO nanoflakes. d–f) shows an enlargement of the red boxed area from a–c), respectively. Blue arrows indicate GO nanoflakes.

performed an in-depth proteome analysis on biological samples. Untreated Aβ42-expressing cells were analyzed alongside those treated with 50 or 100 μg mL^{-1} of GO nanoflakes. Analyses were performed at three time points: day 1 (D1, growth phase), day 2 (D2, beginning of stationary phase), and day 4 (D4, late stationary phase) during the chronological aging experiment (Figure S4, Supporting Information). In total, 2493 proteins were quantified in at least two biological replicates under at least one experimental condition (Data 1, Supporting Information). The range of median coefficient of variation (CV) was between 7% and 14% across all biological replicates, indicating a high degree of reproducibility (Figure S5a, Supporting Information). Principal component analysis (PCA) revealed distinct protein expression profiles in the untreated Aβ42 strain and strains treated with different concentrations of GO nanoflakes (Figure S5b, Supporting Information). The impact of the GO nanoflakes treatment on the proteome of the Aβ42 strain seemed to be concentration dependent. With the treatment of 100 μg mL^{-1} of GO nanoflakes, the numbers of differentially expressed proteins were two times >50 μg mL^{-1} GO nanoflakes treatment (Figure S6, Supporting Information). Of note, treatment with the higher dose of GO nanoflakes influenced not only more proteins but also overall more biological processes (FDR < 0.05, Figure S7, S8, Supporting Information).

2.4. GO Nanoflakes Boost the Capacity of Aβ42-Expressing Yeast Cells to Handle ER Stress

Our previous transcriptome study has shown that accumulation of Aβ42 aggregates can trigger a strong ER stress, resulting in activation of unfolded protein response (UPR).[15b] Induction of UPR tends to enhance protein folding/refolding and degrada-

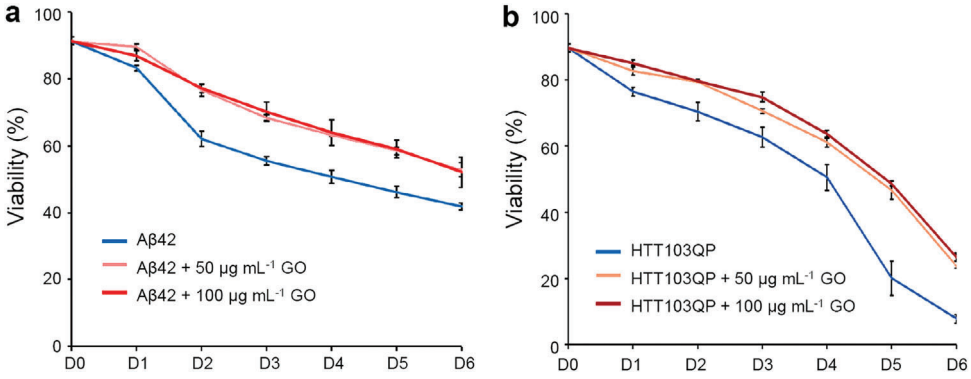

Figure 2. GO nanoflakes reduce Aβ42 and HTT103QP cytotoxicity. Survival of the a) Aβ42 strain and b) the HTT103QP strain with either 50 or 100 μg mL^{-1} of GO nanoflakes treatment following CLS. Viability is shown as the fraction of PI negative cells identified by flow cytometry. 5000 cells were measured per sample with results shown as average values ± SD from three biological replicates.

tion, and repress protein biosynthesis in order to restore ER homeostasis. Nevertheless, the activated UPR fails to buffer the misfolded protein load generated by Aβ42 and leads to cellular dysfunction.[15b] In this study, Aβ42 strain treated with GO nanoflakes exhibited an increased capacity to deal with the ER stress. UPR-related protein processes (triggered by ER stress) including protein degradation and protein folding were activated in GO-treated cells, suggesting that the treated cells are more capable of reducing the misfolded protein burden generated by Aβ42 aggregates (**Figure 3**a; Figure S9, Supporting Information). To confirm this hypothesis, we stressed GO-treated cells with L-azetidine-2-carboxylic acid (AZE), which is an analog of L-proline. AZE is identical to proline except that its ring contains four members instead of five (Figure 3b). This structural difference results in protein misfolding, aggregation, and ER stress when AZE substitutes proline during protein biosynthesis.[20] The control strain, which contains only the promoter and terminator sequences, was treated with 50 and 100 μg mL^{-1} GO, respectively (Figures S10 and S11, Supporting Information). In the untreated control strain, the 2.5 mM AZE treatment strongly decreased cellular viability. By contrast, cells treated with both concentrations of GO nanoflakes were better protected from the effects of AZE (Figure 3c). The cellular viability was further quantified by colony forming units (CFU) counting. Around 400 cells were plated on selective plates and colonies were scored after 3 days incubation. Viability (%) is shown as the CFU counting divided by the number of plated cells. The fractions of viable cells were 2.3% in the control strain without GO, comparing to 25.1% and 41.3% with 50 and 100 μg mL^{-1} GO treatment, respectively ($p < 0.05$, Figure 3d). When the AZE concentration was further increased to 5 mM, causing higher cellular stress, the GO treatment could still improve cell survival ($p < 0.05$, Figure S12, Supporting Information). Another component of reducing ER stress in GO-treated Aβ42 strain seems to be achieved by reducing protein translation. In the GO treated cells, the pathways involved in ribosome biogenesis/assembly, protein translation, and rRNA processing were significantly repressed compared to the non-treated strains (FDR < 0.05, Figure S7, Supporting Information). Suppression of translational activity can prevent an overload of the ER with newly synthesized proteins.[21] In order to explore the underlying transcriptional regulatory response upon GO nanoflakes treatment, the affected transcription factors (TFs) were identified by integrating the proteomics data with the TFs network. Affected TFs were scored by the modulation of protein expression. In total, nine reporter TFs were identified as downregulated, and seven out of them were associated with regulation of transcription processes, such as transcription of ribosomal protein and biogenesis genes, transcription initiation and elongation (p-adj < 0.05, Figure S13, Supporting Information). This is consistent with the gene set enrichment analysis (GSEA) results (FDR < 0.05, Figure S7, Supporting Information). Among other pathways, endocytosis was observed to be more active in the Aβ42 strain treated with 100 μg mL^{-1} GO nanoflakes (Figures S8 and S14, Supporting Information). This is in line with the previous observations linking endocytosis and AD, as neurons are particularly susceptible to perturbations in the endocytic homeostasis because they continually recycle the neurotransmitters and their receptors.[22] A previous study has highlighted the link between Aβ42 and endocytosis, as a key risk factor for AD pathogenesis in humans.[14] The *SLA1*, one of endocytic factors identified from a yeast genome-wide screen, is shown to suppress the toxicity of Aβ oligomers in glutamatergic neurons of *Caenorhabditis elegans* and rat cortical neurons.[14] It was noticed that the Sla1 expression was upregulated in the Aβ42 strain treated with 100 μg mL^{-1} l of GO nanoflakes (p-adj < 0.05, Figure S14, Supporting Information). Overall, these results indicate that treatment with GO nanoflakes may increase the cellular capacity to cope with misfolded protein stress.

2.5. GO Nanoflakes Activate the Metabolism and Improve Redox Homeostasis in Aβ42-Expressing Yeast Cells

Increased oxidative stress is known to be implicated in the pathogenesis of AD.[23] Brain cells are prone to oxidative stress due to their higher energy demand and lower antioxidant activity, suggesting the crucial role of redox homeostasis. The cellular redox state is determined by the ratios between reduced and oxidized forms of redox cofactors, such as nicotinamide adenine dinucleotide phosphate (NADP) and nicotinamide adenine dinucleotide (NAD). These redox cofactors are generated primarily in carbohydrate metabolism. The GSEA showed that most enzymes involved in central carbohydrate metabolism including glycolysis and pentose phosphate pathway (PPP) were significantly upregulated after GO treatment compared to the Aβ42 strain without treatment (p-adj < 0.05, Figure 3e). Glycolysis and PPP[24] are important for generation of NADH (reducing power) and NADPH (reducing power), respectively. In the Aβ42 strain, 50 μg mL^{-1} of GO nanoflakes treatment resulted in a significant ($p < 0.05$) increase of the NADPH/(NADPH + NADP$^+$) ratio (Figure 3f) and NADH/(NADH + NAD$^+$) ratio on day 1 (Figure 3g). Along with the increased glycolysis and PPP, the amino acid biosynthesis (Figure S15, Supporting Information) and the biosynthesis of purines and pyrimidines (Figure S16, Supporting Information) were also activated by the GO nanoflakes treatment. Besides being building blocks of nucleic acids, most purine and pyrimidine nucleotides also represent sources of energy that drive important cellular reactions.[25] The cellular pathways related to oxidative stress, oxidation–reduction processes, and redox homeostasis were also boosted by the GO nanoflakes treatment in Aβ42 strain (FDR < 0.05, Figure S7, Supporting Information). Affected TF analysis showed that proteins regulated by four TFs were significantly upregulated in GO nanoflakes treated Aβ42 strain, and two out of them were stress-responsive transcriptional activators (p-adj < 0.05, Figure S13, Supporting Information). In particular, the proteins involved in thioredoxin and glutathione systems, critical antioxidant systems in cells, were significantly overexpressed in the GO nanoflakes-treated Aβ42 strain (Figure 3h). Thioredoxin (TRX) and glutaredoxin (GRX) are small heat-stable proteins with redox-active cysteines that facilitate the reduction of other proteins.[26] The mRNA levels of human *TXN* (ortholog of yeast *TRX1*) have found to be significantly lower in the cerebellum of AD patients compared to normal controls (p-adj < 0.01, Figure S17, Supporting Information). Study showed that deregulation of TRX1 antioxidant system may contribute to the increased oxidative stress in the AD pathogenesis and overexpression of *TRX1* can protect cells from Aβ toxicity.[27] The expression level of Trx1 protein was significantly increased in Aβ42 strain

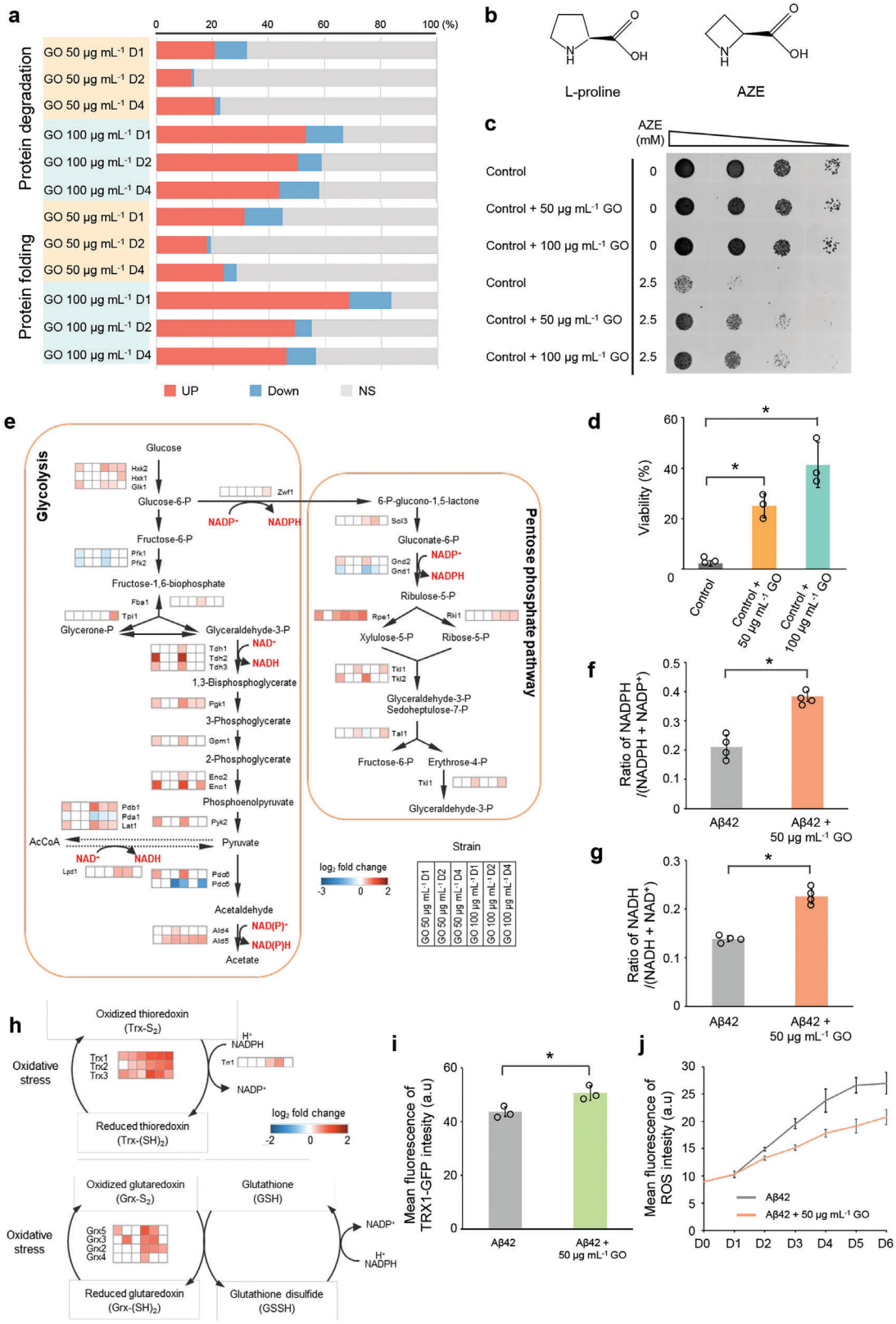

Figure 3. GO nanoflakes activate cellular capacity to deal with misfolded proteins and oxidative stress. a) For protein degradation and folding processes, the percentages of proteins that are either higher (red), lower (blue), or not significantly (NS, gray) differentially expressed in Aβ42 strain treated with 50 and 100 μg mL^{-1} of GO nanoflakes during D1, D2, and D4 are shown. b) The structures of L-proline and AZE. c) Ten-fold serial dilutions of the control strain after 3.5 h of 2.5 mM AZE treatment. d) CFU measurement of cellular viability after 3.5 h of 2.5 mM of AZE treatment ($n = 3 \pm$ SD). e) Fold changes

treated with 50 μg mL^{-1} of GO nanoflakes compared to untreated Aβ42 strain ($p < 0.05$, Figure 3i). To test whether these specific proteome changes translate into a change in the cellular levels of ROS, the ROS levels were investigated in the Aβ42 strain treated with 50 μg mL^{-1} of GO nanoflakes following the chronological aging. The GO nanoflakes-treated cells were found to have significantly lower levels of ROS throughout the time span compared to untreated cells ($p < 0.05$, Figure 3j). Taken together, these results indicate that GO nanoflakes treatment can improve redox homeostasis, which helps the overall cell response to oxidative stress.

2.6. GO Nanoflakes Suppress Formation of Aβ42 Aggregation

Aβ42 is prone to forming various aggregates, including dimers, trimers, tetramers, higher molecular weight oligomers, and fibrils. Among them, the soluble high molecular weight oligomers appear to be the most toxic species.[28] Reducing levels of oligomeric Aβ has been shown to improve memory in plaque-bearing mice models.[29] Several in vitro studies have indicated that hydrophobic interactions between GO nanoflakes and Aβ42, can suppress the formation of Aβ aggregates.[6,30] Next, whether this process may account for the reversal Aβ42 phenotype describe above. To investigate whether the internalized GO nanoflakes interact with intracellular Aβ42, sectioned cell samples were labeled with Aβ-specific antibody prior to TEM analysis. In the non-treated strain, immuno-TEM images revealed enrichment of labeled Aβ42 aggregates inside the vacuoles (**Figure 4**a,d,g), in accord with a previous study that showed the accumulation of Aβ42 inside lysosomes of neuroblastoma (SH-SY5Y) cell line.[31] A closer examination revealed the enrichment of Aβ42 by GO nanoflakes inside vacuoles. Significantly more Aβ42 signals were accumulated around the GO nanoflakes, indicating a degree of interaction between them (Figure 4b,e,h,c,f,i). The number of labeled Aβ42 signals per cell area was quantified from the immune-TEM pictures in the cells. This suggested that GO treatment significantly reduced the number of Aβ42 signals compared to the untreated Aβ42 strain ($p < 0.05$, Figure 4j). To check this hypothesis, we performed a western blot analysis of the intracellular soluble Aβ42 including monomers and all states of aggregates, with and without GO nanoflakes treatment. The GO treatment reduced total amount of Aβ42 in the strain ($p < 0.05$, Figure 4k; Figure S18, Supporting Information), especially the high molecular weight oligomers were significantly decreased in a dose-dependent manner ($p < 0.05$, Figure 4k,l). This is in accord with the immune-TEM data (Figure 4j) and improved cellular viability (Figure 2a), and can probably be correlated to the phenomenon observed in plaque-bearing mice models, which showed reducing levels of oligomeric Aβ improve mice memory.[29] Next, we asked whether this suppression of the high molecular weight Aβ42 aggregates can fully account for the observed reduction of the Aβ42 phenotype observed in our yeast model. Our proteomics data suggested that cells overexpressed the machinery required to deal with ER stress and oxidative stress upon GO treatment. To check whether this boosting of natural stress defenses can proceed independently from Aβ42 aggregates, we treated control cells with GO. In these cells, the GO treatment had the same beneficial effects, the capacity to deal with oxidative stress was improved (Figure S19, Supporting Information) and cellular viability was increased during chronological aging (Figure S20, Supporting Information). Hence, we concluded that GO acts by two independent pathways in mitigating toxicity of Aβ42 in yeast: 1) It acts directly, via suppressing Aβ42 aggregation and 2) it acts indirectly, boosting cellular capacity to deal with misfolded proteins and oxidative stress by a presently unknown mechanism, leading to transcriptional activation of specific stress response genes.

2.7. GO Reduces Cytotoxicity of Human HTT103QP Protein Expressed in Yeast

The formation of misfolded protein aggregates is a common hallmark of many neurodegenerative diseases (ND). To investigate the specificity of the GO nanoflakes effects, we tested their impact on another yeast model of a ND, namely the yeast that expresses human HTT103QP protein, a hallmark of HD. HD is an autosomal dominant ND caused by the expansion of CAG trinucleotide repeats, which encode the polyglutamine (polyQ) expansion in the Huntingtin (HTT) protein. In yeast model, polyQ expansion beyond 47 or more can cause HTT protein to misfold and aggregate, and lead to cytotoxicity, that are similar to the phenotypes observed in HD patients.[32] The HD model we used in this study was constructed with 103 polyQ expansion with C-terminal GFP fusion.[13] Microscopy showed that HTT103QP proteins were present in different sizes of punctate patches (Figure S21, Supporting Information). The cellular viability of HTT103QP strain without and with GO nanoflakes treatment was evaluated following chronological aging. The treatment of GO nanoflakes significantly improved cellular viability in the HTT103QP strain as well (Figure 2b). At present we cannot say whether the protective effect is due primarily to the augmented stress response provoked by GO, or GO is also capable of suppressing HTT103QP aggregation. It is plausible to presume that GO might function as a general chaperon, preventing misfolding of various proteins. To test this, we set up an in vitro assay with α-amylase as a reporter. The enzyme was denatured at 55 °C for 20 min, which reduced its enzyme activity by 55% (Figure S22a, Supporting Information). Next, the partially denatured enzyme was incubated with GO nanoflakes. The treatment was failed to preserve or restore the α-amylase activity, indicating that it probably cannot act as a

in the expression of proteins that encode glycolysis and pentose phosphate pathway (PPP). f) Ratio of NADPH/(NADPH + NADP$^+$) in the Aβ42 strain without or with 50 μg mL^{-1} GO nanoflakes treatment on Day 1 ($n = 4 \pm$ SD). g) Ratio of NADH/(NADH + NAD$^+$) in the Aβ42 strain without or with 50 μg mL^{-1} GO nanoflakes treatment on Day 1 ($n = 4 \pm$ SD). h) Fold changes in the expression of proteins in redox homeostasis including thioredoxin pathway and glutathione–glutaredoxin system. i) Flow cytometry analysis of GFP-tagged TRX1 expression in the Aβ42 strain without and with 50 μg mL^{-1} GO nanoflakes treatment on Day 1 ($n = 3 \pm$ SD). j) Flow cytometry analysis of intracellular ROS in the Aβ42 strain without and with 50 μg mL^{-1} GO nanoflakes ($n = 3 \pm$ SD). Asterisks (*) from d) indicate significant differences compared to control strain without GO nanoflakes treatment ($p < 0.05$). Asterisks (*) from f,g,i) indicate significant differences compared to Aβ42 strain without GO nanoflakes treatment ($p < 0.05$). All comparison in a,e,h) is in the Aβ42 strain between GO nanoflakes treatment and without (p-adj < 0.05 according to Benjamini–Hochberg method).

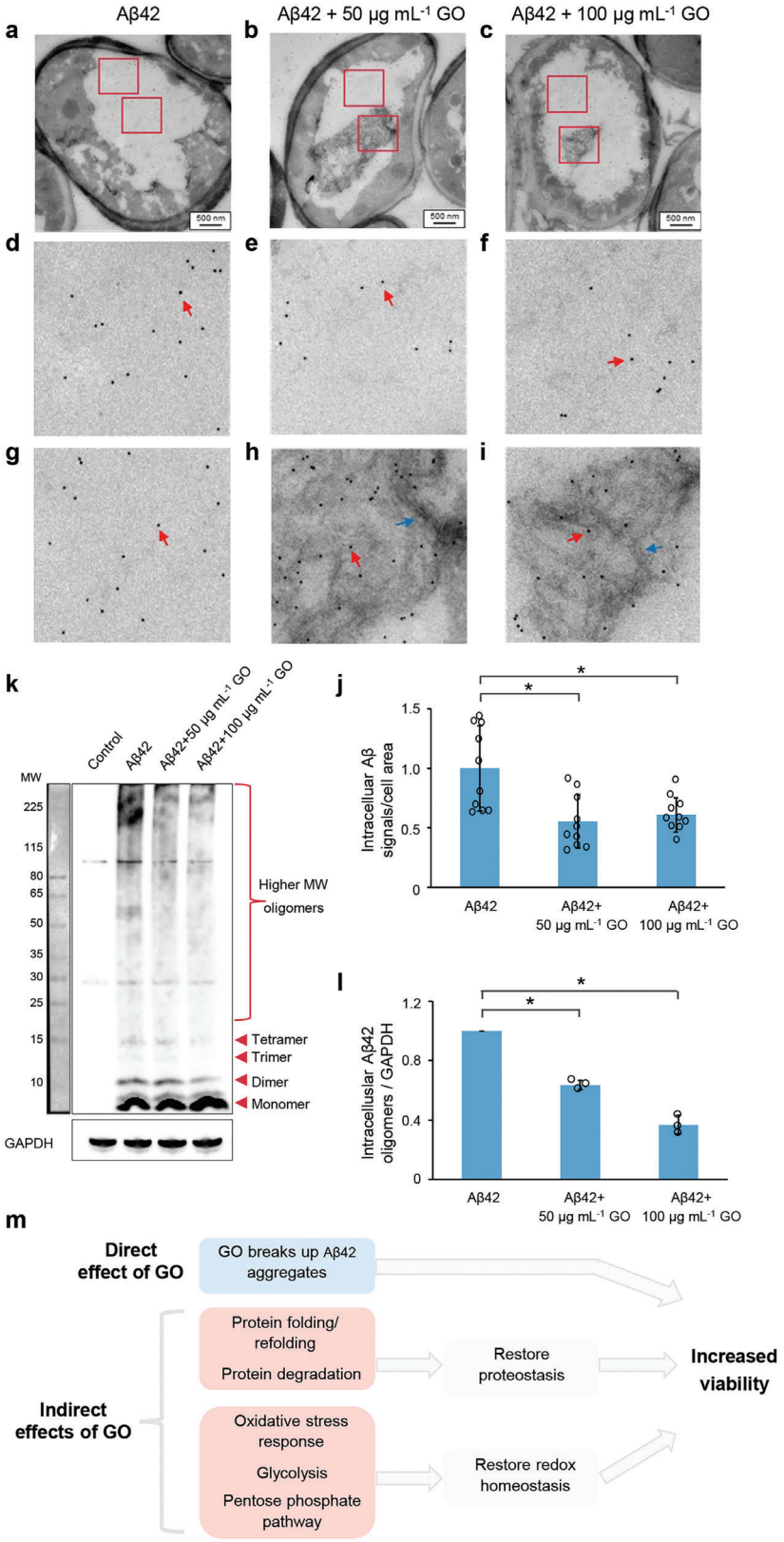

Figure 4. GO nanoflakes suppress formation of Aβ42 aggregation. Immuno-TEM images of a) Aβ42 strain, b) Aβ42 strain treated with 50 μg mL^{-1} of GO nanoflakes, and c) Aβ42 strain treated with 100 μg mL^{-1} of GO nanoflakes. d–f) shows an enlargement of the upper red boxed area from a–c), respectively. g–i) shows an enlargement of the lower red boxed area from (a–c), respectively. Blue arrows indicate GO nanoflakes. Red arrows indicate the immunogold labeled Aβ42 aggregates. j) Quantitative analysis of intracellular Aβ aggregates from immune-TEM images. The value of intracellular

general chaperone ($p > 0.05$, Figure S22b, Supporting Information). From this, we concluded that GO nanoflakes are not likely to act as a chaperon on all misfolded proteins directly but are likely to reduce the global protein misfolding burden caused by aggregation of Aβ42 and HTT103QP in yeast.

3. Conclusion

The potential of GO nanoflakes as a treatment for AD has been previously suggested on a mouse model of AD.[9a] Previous in vitro studies indicated that GO nanoflakes could promote disassembly of Aβ42 aggregates.[33] Using the yeast model for Aβ42 expression, which was previously shown to be a good model for Aβ toxicity,[13,15] we demonstrate that the treatment with GO nanoflakes can diminish the Aβ toxicity phenotype. The proposed mechanism, supported by our evidence, proceeds along two lines. It starts with effective internalization of GO nanoflakes with 90 nm in diameter. Internalized GO then boosts cellular machinery for coping with protein misfolding and oxidative stress, which indirectly mitigates Aβ42 toxicity. The second line of action proceeds via specific depletion of intracellular high molecular weight Aβ42 aggregates, triggered by GO (Figure 4m). Interestingly, the beneficial effects of GO nanoflakes seem to extend also to a HD yeast model, suggesting that GO nanoflakes can contribute to rational design of future strategies for attenuating neurodegenerative pathology.

4. Experimental Section

Characterization of GO: The size of GO nanoflakes was determined using DLS on a Zetasizer nano instrument (Malvern Panalytical Ltd., Malvern, UK) at room temperature. Plastic cuvettes were utilized, and the concentration of the samples was set at 10 µg mL^{-1}. Water was employed as the dispersant, with a refractive index and viscosity of 1.330 and 0.8872 centipoise, respectively. The Raman spectra were obtained using a Raman microscope with a 638 nm laser (Horiba Raman XploRA microscope). The instrument was equipped with a 50× objective, a 532 nm laser, and a 600 g mm^{-1} grating. Each spectrum was recorded within the range of 500–3000 cm^{-1}, with ten accumulations per spectrum and an integration time of 0.5 s.

Strain, Medium, and Culture Conditions: All strains were derived from the laboratory strain CEN.PK113-11C (*MATa his3Δ1 ura3-52 MAL2-8c SUC2*). The Aβ42 strain (*XI-3*::*GPDp-Aβ42-CYC1t XII-5*::*GPDp-Aβ42-CYC1t*) harboring two copies of Aβ42 genes[13] and control strain (*XI-3*::*GPDp-CYC1t XII-5*::*GPDp-CYC1t*) containing only the promoter and terminator sequences[13] were used in this study. The HTTP103QP and its control strain harbored p416 GPD-HTTP103QP-GFP and p416 GPD-HTTP25QP-GFP plasmids, respectively.[13] The TRX1-GFP strain was constructed using homologous recombination-based method. The *TRX1* gene and its 500 bp of upstream and downstream homologous arms were amplified from CEN.PK113-11C genomic DNA. The GFP and kanMX fragments were amplified from p416 GPD-GFP and pUG6 vectors, respectively. The TRX1 upstream + TRX1 + GFP + kanMX + TRX1 downsteam cassette was generated via fusion PCR and transformed into CEN.PK113-11C to replace endogenous *TRX1* sequence. The transformants were selected on YPD-G418 plates containing 10 g L^{-1} yeast extract, 20 g L^{-1} peptone, and 20 g L^{-1} glucose, and 200 mg L^{-1} G418. mediYeast cells were cultured in Delft um (pH 6.0), containing (L^{-1}) 7.5 g $(NH_4)_2SO_4$, 14.4 g KH_2PO_4, 0.5 g $MgSO_4 \cdot 7H_2O$, 100 mg histidine, 100 mg uracil, and 20 g glucose. After autoclavation, 2 mL trace metals and 1 mL vitamins solutions were added to the medium.[34] Yeast cells were cultivated at 30 °C with 200 rpm agitation. GO nanoflakes dispersed in water were purchased form from graphene supermarket (https://graphene-supermarket.com/). GO nanoflakes were then diluted using sterile water and different sizes were produced by different time of sonication duration. The sizes of 250, 220, and 90 nm of GO nanoflakes were achieved by sonication for 10, 30, and 180 min, respectively. GO nanoflakes were added to culture medium at early exponential phase ($OD_{600} \approx 1$) to final concentrations of 50 and 100 µg mL^{-1}, respectively. Soon after addition of GO nanoflakes, the culture medium was sonicated for 45 s using probe sonicator (10% of amplitude) to achieve a homogeneous dispersion of GO nanoflakes in the solution.

SEM: Aβ42 and control strains were inoculated in 5 mL of culture medium in 50 mL Falcon tube with an initial OD_{600} of 0.1. In the early exponential phase ($OD_{600} \approx 1$), either 50 or 100 µg mL^{-1} of GO nanoflakes were added to the culture medium. After 48 h of GO nanoflakes treatment, cells were fixed overnight with 3% glutaraldehyde. The fixed cells were dehydrated with a series of increasing ethanol concentration (40%, 50%, 60%, 70%, 80%, 90%, and 100%) for 10 min each. Thin films were prepared by using dehydrated yeast cells on cover glass and dried overnight at room temperature. The dried samples were sputter coated with gold (5 nm) before imaging. The SEM images were acquired by using JEOL JSM 6301F (Carl Zeiss AG, Jena, Germany).

TEM: Samples were prepared as described in SEM experiment. Cells were fixed in 2% glutaraldehyde (EM grade, Electron Microscopy Sciences) in cacodylate buffer overnight at 4 °C and digested with Zymolyase (ZYMO research) at 37 °C for 25 min to remove cell wall. Post-fixation was performed in 1% osmium tetroxide and 1% potassium ferricyanide (III) for 30 min at room temperature. To enhance contrast of proteins, *en-bloc* staining with 1% aqueous uranyl acetate was performed at room temperature for 1 h. Samples were subsequently dehydrated in increasing ethanol solutions (30%, 50%, 70%, 85%, 95%, 100%), 10 min for each step. Gradient infiltration with epoxy hard plus resin (Electron Microscopy Sciences) was performed at 25%, 50%, 75%, and 100% of resin in ethanol solution, 10 min for each step. Polymerization was performed at 60 °C for 16 h. Ultrathin sections at 70 nm thick were obtained using a Leica EM UC6 ultramicrotome (Leica) and collected on formvar-coated copper mesh nickel grids. Images were acquired on a transmission electron microscope (Talos L120C with 4k × 4k Ceta CMOS camera, Thermo Fisher Scientific).

Viability Assay and ROS Staining: Cell viability was measured by PI staining (Thermo Fisher Scientific). PI stains cells with disintegrated plasma membranes as red color, which are considered as dead cells.[35] 0.5 OD_{600} of cells were harvested and resuspended in 1 mL of PBS buffer. Cells were stained with 0.5 µg mL^{-1} of PI at room temperature for 20 min in the dark. Red fluorescence (690/50 filter) was analyzed after excitation by a 488 nm laser using a Guava flow cytometer (Merck). Viability was shown as the fraction of PI negative cells. Intracellular ROS levels were detected by dihydrorhodamine 123 (DHR123, Sigma-Aldrich). DHR123 could passively diffuse across plasma membrane and be oxidized to rhodamine 123, which exhibits green fluorescence. For staining, 0.5 OD_{600nm} of cells were taken and incubated with 5 µm DHR123 dye in the 50 mM sodium citrate buffer (pH 5.0) for 30 min at room temperature in the dark. Green fluorescence (525/30 filter) was analyzed using Guava flow cytometer (Merck).

Aβ signal was calculated by the ratio of the number of labeled Aβ signals to the cell area ($n = 10 \pm$ SD). k) Western blot analysis of Aβ42 expression without and with GO nanoflakes treatment. GAPDH is used as a loading control. l) Relative intensity of Aβ42 oligomers in Aβ42 strain. The intensity of Aβ42 oligomers was quantified from (k) and normalized to GAPDH ($n = 3 \pm$ SD). Asterisks (*) from (j,l) indicate significant differences compared to Aβ42 strain without GO nanoflakes treatment ($p < 0.05$). m) Schematic overview of the effects of GO nanoflakes treatment on Aβ42 strain. GO nanoflakes directly interact and break up Aβ42 aggregates to reduce its cytotoxicity. Additionally, GO nanoflakes cause the proteome rearrangement to improve viability through restoration of proteostasis and redox homeostasis.

Result was shown as the mean fluorescence intensity. In total, 5000 cells were analyzed for each sample.

Sample Preparation for Proteomics Analysis: 20 mL of Aβ42-expressing cells were cultivated in 100 mL shake flask to early exponential phase (OD_{600} ≈1). GO nanoflakes were added to culture medium to final concentrations of 50 and 100 µg mL^{-1}, respectively. This time point was designated as day 0. 10 OD_{600} of cells were collected at day 1, day 2, and day4. Three biological replicates were processed for each time point and for each condition. Cells were washed once with ice-cold PBS buffer, snap-frozen in liquid nitrogen and stored at −80 °C. Cell lysis was performed by resuspending the cell pellet in lysis buffer containing 8 M urea, 75 mM NaCl, 50 mM Tris-HCl (pH 8.0) and complete protease inhibitor cocktail (Roche). Using 425–600 µm glass beads, the cell suspension was subjected to bead beating at 4 °C (five cycles of 2 min pulses of 60 Hz with 1 min rest between each cycle). Cells were then spun at 13,400 rpm for 30 min at 4 °C to obtain a clear cell lysate. Proteins were precipitated using eight volumes of ice-cold acetone and one volume of ice-cold methanol to the resulting cell lysate, followed by wash with ice-cold 80% acetone. The resultant protein pellet was dissolved in 10 mM Tris buffer at pH 8.0 containing 6 M urea and 2 M thiourea. Protein concentrations were estimated by Bradford (BioRad). Subsequently, 5 mM dithiothreitol was added to 15 µg of total protein to initiate the digestion protocol and the samples were incubated for 45 min at 57 °C. The lysates were cooled and subsequently treated with 15 mM iodoacetamide for 45 min in the dark at room temperature. Further incubation with 5 mM dithiothreitol for 15 min at 57 °C was carried out. The lysates were next diluted 5.3 times with 50 mM Tris (pH 8.0). Lysyl Endopeptidase (Wako) at a 1:50 enzyme to protein ratio was added and the samples were incubated for 3 h at room temperature with gentle shaking. After 3 h, trypsin (Thermo Scientific) was added to the samples at the same ratio, and they were further incubated for 16 h. The reaction was arrested by acidifying the samples with 10% trifluoroacetic acid. The resultant peptide mixtures were next desalted using C18 stage-tips.[36]

NanoLC-MS/MS and Data Analysis: After desalting using C18 Stagetips, 500 ng of peptide mixtures were loaded on an Easy-nLC 1200 system (Thermo Fisher Scientific) coupled to a quadrupole Orbitrap Exploris 480 mass spectrometer (Thermo Fisher Scientific) as described previously[37] with slight modifications. 20 cm analytical column (75 µm ID PicoTip fused silica emitter, New Objective) was packed in-house with ReproSil-Pur C18-AQ 1.9 µm resin (Dr Maisch GmbH). Peptides were separated using a 57 min segmented gradient from 10-33-50-90% of HPLC solvent B (80% acetonitrile in 0.1% formic acid) in HPLC solvent A (0.1% formic acid) at a flow rate of 200 nL min^{-1}. The mass spectrometer was operated in data-dependent mode, collecting MS spectra in the Orbitrap mass analyzer (60000 resolution, 300–1750 m/z range) with an automatic gain control (AGC) set to standard and a maximum ion injection time set to automatic. The 20 most intense precursor ions were sequentially fragmented with a normalized collision energy of 28 in each scan cycle using higher energy collisional dissociation (HCD) fragmentation. In all measurements, sequenced precursor masses were excluded from further selection for 30 s. MS/MS spectra were recorded with a resolution of 15 000, whereby fill time was set to automatic. Measurements were done in three technical replicates.

Acquired MS spectra were processed with the MaxQuant software suite (version 1.6.7.0),[38] integrated with an Andromeda search engine. Database search was performed against a target-decoy database of Saccharomyces cerevisiae S288c downloaded from UniProt (taxonomy ID 559 292), containing 6749 protein entries, and additionally including also 246 commonly observed laboratory contaminants. Endoprotease Trypsin/P was set as the protease with a maximum missed cleavage of two. Carbamidomethylation (Cys) was set as a fixed modification. Label free quantification was enabled with a minimum ratio count of two. A false discovery rate of 1% was applied at the peptide and protein level individually for filtering identifications. All other parameters were maintained as default.

Proteomics Data Analysis: Differential protein expression analysis was performed with the LFQ Analyst web application[39] using the MaxQuant "proteinGroups.txt" as the input file. Only protein groups having measured intensity values for at least two replicates of at least one experimental condition were kept in this analysis. The data was analyzed using the Perseus-type ("Missing not At Random") imputation method, the "paired" test option and the Benjamini Hochberg FDR type correction. PCA and Sample Coefficient of Variation plots were generated from the LFQ Analyst output graphics. The Report GO terms and reporter TFs were generated from the Platform for Integrative Analysis of Omics (PIANO)[40] *R* package with information from Saccharomyces Genome Database (https://www.yeastgenome.org/). The DAVID Database (https://david.ncifcrf.gov/) was applied to analyze functional enrichment of biological process and KEGG pahtway. Heatmaps of significantly changed proteins were generated from the pheatmap *R* package.

AZE Experiment: The control strain was grown to early exponential phase (OD_{600} ≈1) and treated with GO nanoflakes for 3 h at concentrations of 50 and 100 µg mL^{-1}, respectively. To assess the cell resistance to protein misfolding stress, AZE (Sigma-Aldrich) was added to the culture medium to final concentration of 2.5 mM. After 3.5 h of cultivation, 0.2 OD_{600} of cells were collected and resuspended in 1 mL of sterile H_2O. For spot-assay, cells were serially diluted (10^{-1}, 10^{-2}, and 10^{-3}) and spotted on Delft agar plates. Cell viability was evaluated by CFU counting. Around 400 cells were plated on Delft agar plates and colonies were scored after 3 days incubation. Viability was shown as the CFU divided by the number of plated cells. Results are from biological triplicates.

NADP(H) and NAD(H) Measurements: NADP(H) and NAD(H) levels were determined by the $NADP^+$/NADPH Quantification Kit (Sigma) and the NAD^+/NADH Quantification Kit (Sigma). Cells were collected at day 1 after 50 µg mL^{-1} of GO nanoflakes treatment. 19 mL of pre-chilled methanol was immediately added to cells to quench cellular metabolism. Then cells were centrifuged at −10 °C, 4000 g for 4 min. After removing the supernatant, cell pellets were freeze-dried for 2 h with 0.1 mbar pressure at −80 °C. The dried cell pellet was resuspended in 500 µL of extraction buffer (from the kit) and transferred to 2 mL screw-top tubes containing 0.2 g of lysis beads (425–600 µm diameter, Sigma). Cells were lysed via the Precellys Evolution Homogenizer (Bertin technologies), 5 m/20 s/4 rounds followed by 1 min intervals on ice. The lysed samples were centrifuged at 0 °C, 14 000×g for 10 min. Supernatant was further filtered by a 10 kDa cut-off spin filter (Thermo Fisher Scientific) to remove enzymes in the lysates. Colorimetric measurement of NADP(H) and NAD(H) was performed following the manufacturer's instructions (Sigma).

Analysis of TXN Gene Expression in the Human Cerebellum: The brain expression datasets that were deposited in the GeneNetwork website (http://www.genenetwork.org) were analyzed. Approximately 400 AD patients and 170 age-, gender-, and postmortem interval-matched normal controls were enlisted in the study. The cerebellum was profiled on a custom-made Agilent 44 K microarray. The mRNA expression levels of *TXN* were analyzed to define its association with AD. Differential *TXN* expression between AD patients and normal control were identified using a Mann–Whitney test.

Immuno-TEM: Samples were prepared as described in SEM experiment. Cells were fixed with 4% paraformaldehyde and 0.5% glutaraldehyde (EM grade, Electron Microscopy Sciences) in 0.1 M phosphate buffer (pH 7.0) overnight at 4 °C. After fixation, cells were embedded in 10% of gelatin at 37 °C for 10 min. Then cells were incubated in 2.3 M sucrose overnight at 4 °C and ready for sectioning. Sections (70 nm) were collected on carbon/formvar coated mesh nickel grids and immune-labeled with the monoclonal anti-Aβ primary antibody (6E10, 1:10 dilution, Covance), followed by anti-mouse IgG conjugated with 10 nm gold beads (1:50 dilution, Abcam). Images were acquired on a transmission electron microscope (Talos L120C with 4k × 4k Ceta CMOS camera, Thermo Fisher Scientific).

Protein Extraction and Western Blot: Aβ42 strain was inoculated in 20 mL of culture medium with an initial OD_{600} of 0.1 in 100 mL shake flask. In the early exponential phase (OD_{600} ≈ 1), either 50 or 100 µg mL^{-1} of GO nanoflakes were added to the culture medium. After 48 h, 5 OD_{600} of cells were harvested at 4 °C for 5 min (2000 g) and resuspended in 200 µL of pre-chilled lysis buffer, which contained 150 mM NaCl, 50 mM HEPES (pH 7.5), 2.5 mM EDTA, 2 µL Triton X-100, and protease inhibitors (Roche). Samples were transferred into 2 mL lysing Matrix tubes with 200 µL of acid-washed glass beads (425–600 µm, Sigma-Aldrich) and homogenized at speed 6.5 m s^{-1} for 45 s, three cycles, using FastPrep-24 (MP Biomed-

icals). Samples were cooled down on ice for 5 min between each cycle. Then samples were mixed with 200 µL of 2 × SDS sample buffer containing 20% glycerol, 100 mM Tris-HCl (pH 6.8), 4% SDS, 0.02% bromophenol blue, 20 µL of β-mercaptoethanol, and boiled at 70 °C for 10 min. To remove cell debris, samples were centrifuged at 21 000 g for 10 min. Then supernatants were collected, and protein concentration was measured using Pierce BCA Protein Assay Kit (Thermo Fisher Scientific). Western blot was performed as described previously.[15a] Aβ42 levels were detected by anti-Aβ primary antibody (6E10, mouse monoclonal, 1:1000 dilution, Covance) and anti-mouse-HRP (1:2000 dilution, Dako). GAPDH levels were identified as a loading control by anti-GAPDH primary antibody (mouse monoclonal, 1:2000 dilution, Santa Cruz) and anti-mouse-HRP (1:4000 dilution, Dako). Protein bands were quantified by Image lab software 6.1.

Heat Resistance Assay of α-Amylase: A commercial α-amylase from *Aspergillus oryzae* (Sigma-Aldrich) was prepared into 4 U mL^{-1} and subjected to heat resistance assay. The α-amylase activity was measured by α-amylase assay kit (K-CERA, Megazyme) as described previously.[41] To determine the time of heat treatment, 4 U mL^{-1} α-amylase was incubated at 55 °C for 0, 5, 10, 15, 20, and 30 min. The following heat resistance assay was performed by 55 °C for 20 min. To determine the effect of GO to α-amylase upon heat treatment, 4 U mL^{-1} α-amylase was incubated at 55 °C for 20 min with GO in 0, 50, and 100 µg mL^{-1}. As control, another 4 U mL^{-1} α-amylase was mixed with GO in 0, 50, and 100 µg mL^{-1}, and the activity was measured immediately. All the reactions were diluted 1:20 by Extraction Buffer solution (included in α-amylase assay kit) to measure the activity.

Statistical Analysis: Significance of differences was determined as mean ± standard deviation (SD) using a two-tailed student *t*-test. Biological triplicates were analyzed unless specified explicitly. Statistical significance was indicated as p value <0.05 unless specified explicitly.

Supporting Information

Supporting Information is available from the Wiley Online Library or from the author.

Acknowledgements

This work was supported by grant from VINNOVA center CellNova (2017-02105) to D.P., Novo Nordisk Foundation (20CC0035580) and Marie Skłodowska-Curie grant (955626) to I.M. and Vetenskapsrådet (2020-04096) to S.P. The authors acknowledge the Centre for Cellular Imaging at the University of Gothenburg and the National Microscopy Infrastructure, NMI (VR-RFI 2016-00968) for providing assistance in transmission electron microscopy. The authors would like to thank Dr. Mirita Franz-Wachtel at the Proteome Centre Tuebingen, University of Tuebingen for help with the LC-MS/MS analysis.

Conflict of Interest

The authors declare no conflict of interest.

Author Contributions

X.C. and S.P. contributed equally to this work. X.C., S.P., D.P., and I.M. conceived the study. X.C., S.P., L.S., V.R., Z.C., and A.G. performed experiments. X.C., V.R., J.K., and E.S. analyzed the proteomic data. I.M. supervised the whole study and assisted with data analysis. X.C. and I.M. wrote the manuscript. All authors commented on and edited the manuscript.

Data Availability Statement

The data that support the findings of this study are available from the corresponding author upon reasonable request.

Keywords

Alzheimer's disease, amyloid-β, graphene oxide, misfolded protein, oxidative stress

Received: April 12, 2023
Revised: June 18, 2023
Published online:

[1] T. Wyss-Coray, *Nature* **2016**, *539*, 180.
[2] J. Hardy, D. J. Selkoe, *Science* **2002**, *297*, 353.
[3] J. L. Cummings, *N. Engl. J. Med.* **2004**, *351*, 56.
[4] a) R. S. Doody, R. G. Thomas, M. Farlow, T. Iwatsubo, B. Vellas, S. Joffe, K. Kieburtz, R. Raman, X. Sun, P. S. Aisen, E. Siemers, H. Liu-Seifert, R. Mohs, *N. Engl. J. Med.* **2014**, *370*, 311; b) S. Salloway, R. Sperling, N. C. Fox, K. Blennow, W. Klunk, M. Raskind, M. Sabbagh, L. S. Honig, A. P. Porsteinsson, S. Ferris, M. Reichert, N. Ketter, B. Nejadnik, V. Guenzler, M. Miloslavsky, D. Wang, Y. Lu, J. Lull, I. C. Tudor, E. Liu, M. Grundman, E. Yuen, R. Black, H. R. Brashear, *N. Engl. J. Med.* **2014**, *370*, 322.
[5] T. M. Magne, T. de Oliveira Vieira, L. M. R. Alencar, F. F. M. Junior, S. Gemini-Piperni, S. V. Carneiro, L. M. U. D. Fechine, R. M. Freire, K. Golokhvast, P. Metrangolo, P. B. A. Fechine, R. Santos-Oliveira, *J. Nanostruct. Chem.* **2022**, *12*, 693.
[6] M. Mahmoudi, O. Akhavan, M. Ghavami, F. Rezaee, S. M. Ghiasi, *Nanoscale* **2012**, *4*, 7322.
[7] Z. Yang, C. Ge, J. Liu, Y. Chong, Z. Gu, C. A. Jimenez-Cruz, Z. Chai, R. Zhou, *Nanoscale* **2015**, *7*, 18725.
[8] N. Zhang, X. Hu, P. Guan, K. Zeng, Y. Cheng, *J. Phys. Chem. C* **2019**, *123*, 897.
[9] a) F. Chu, K. Li, X. Li, L. Xu, J. Huang, Z. Yang, *Neurochem. Res.* **2021**, *46*, 309; b) J. Zhang, S. Zhu, P. Jin, Y. Huang, Q. Dai, Q. Zhu, P. Wei, Z. Yang, L. Zhang, H. Liu, G. Xu, L. Chen, E. Gu, Y. Zhang, L. Wen, X. Liu, *Theranostics* **2020**, *10*, 11908.
[10] a) D. Botstein, G. R. Fink, *Genetics* **2011**, *189*, 695; b) T. Cervelli, A. Galli, *Genes* **2021**, *12*, 1303.
[11] V. Khurana, S. Lindquist, *Nat. Rev. Neurosci.* **2010**, *11*, 436.
[12] M. A. Findeis, *Pharmacol. Ther.* **2007**, *116*, 266.
[13] X. Chen, B. Ji, X. Hao, X. Li, F. Eisele, T. Nyström, D. Petranovic, *Nat. Commun.* **2020**, *11*, 867.
[14] S. Treusch, S. Hamamichi, J. L. Goodman, K. E. S. Matlack, C. Y. Chung, V. Baru, J. M. Shulman, A. Parrado, B. J. Bevis, J. S. Valastyan, H. Han, M. Lindhagen-Persson, E. M. Reiman, D. A. Evans, D. A. Bennett, A. Olofsson, P. L. DeJager, R. E. Tanzi, K. A. Caldwell, G. A. Caldwell, S. Lindquist, *Science* **2011**, *334*, 1241.
[15] a) X. Chen, D. Petranovic, *FEMS Yeast Res.* **2015**, *15*, fov061; b) X. Chen, M. M. M. Bisschops, N. R. Agarwal, B. Ji, K. P. Shanmugavel, D. Petranovic, *Front. Mol. Neurosci.* **2017**, *10*, 232.
[16] H. Hampel, J. Hardy, K. Blennow, C. Chen, G. Perry, S. H. Kim, V. L. Villemagne, P. Aisen, M. Vendruscolo, T. Iwatsubo, C. L. Masters, M. Cho, L. Lannfelt, J. L. Cummings, A. Vergallo, *Mol. Psychiatry* **2021**, *26*, 5481.
[17] A. L. Anding, E. H. Baehrecke, *Dev. Cell* **2017**, *41*, 10.
[18] S. D. Postnikoff, T. A. Harkness, *Methods Mol Biol* **2014**, *1163*, 223.
[19] C. Juan I, O. Stephen G, *Syst. Biol. Alzheimer's Dis.* **2016**, *1303*, 3.
[20] G. Roest, E. Hesemans, K. Welkenhuyzen, T. Luyten, N. Engedal, G. Bultynck, J. B. Parys, *Cells* **2018**, *7*, 239.
[21] D. W. Reid, Q. Chen, A. S. Tay, S. Shenolikar, C. V. Nicchitta, *Cell* **2014**, *158*, 1362.
[22] Y. C. Li, E. T. Kavalali, *Pharmacol. Rev.* **2017**, *69*, 141.
[23] W. R. Markesbery, *Arch Neurol.* **1999**, *56*, 1449.

[24] L.-K. Bertels, L. Fernández Murillo, J. J. Heinisch, *Biomolecules* **2021**, *11*, 725.
[25] B. A. Moffatt, H. Ashihara, *Arabidopsis Book* **2002**, *1*, e0018.
[26] G. J. McBean, M. Aslan, H. R. Griffiths, R. C. Torrão, *Redox Biol.* **2015**, *5*, 186.
[27] S. Akterin, R. F. Cowburn, A. Miranda-Vizuete, A. Jiménez, N. Bogdanovic, B. Winblad, A. Cedazo-Minguez, *Cell Death Differ.* **2006**, *13*, 1454.
[28] a) U. Sengupta, A. N. Nilson, R. Kayed, *EBioMedicine* **2016**, *6*, 42; b) K. Hsiao, P. Chapman, S. Nilsen, C. Eckman, Y. Harigaya, S. Younkin, F. Yang, G. Cole, *Science* **1996**, *274*, 99.
[29] S. Lesné, L. Kotilinek, K. H. Ashe, *Neuroscience* **2008**, *151*, 745.
[30] Y. Jin, Y. Sun, Y. Chen, J. Lei, G. Wei, *Phys. Chem. Chem. Phys.* **2019**, *21*, 10981.
[31] V. Soura, M. Stewart-Parker, T. L. Williams, A. Ratnayaka, J. Atherton, K. Gorringe, J. Tuffin, E. Darwent, R. Rambaran, W. Klein, P. Lacor, K. Staras, J. Thorpe, L. C. Serpell, *Biochem. J.* **2012**, *441*, 579.
[32] R. P. Mason, F. Giorgini, *Prion* **2011**, *5*, 269.
[33] a) P. C. Ke, E. H. Pilkington, Y. Sun, I. Javed, A. Kakinen, G. Peng, F. Ding, T. P. Davis, *Adv. Mater.* **2020**, *32*, 1901690; b) K. P. Loh, D. Ho, G. N. C. Chiu, D. T. Leong, G. Pastorin, E. K. Chow, *Adv. Mater.* **2018**, *30*, 1802368.
[34] N. B. Jensen, T. Strucko, K. R. Kildegaard, F. David, J. Maury, U. H. Mortensen, J. Forster, J. Nielsen, I. Borodina, *FEMS Yeast Res.* **2014**, *14*, 238.
[35] L. C. Crowley, A. P. Scott, B. J. Marfell, J. A. Boughaba, G. Chojnowski, N. J. Waterhouse, *Cold Spring Harb. Protoc.* **2016**, *7*, pdb-prot08716.
[36] Y. Ishihama, J. Rappsilber, M. Mann, *J. Proteome Res.* **2006**, *5*, 988.
[37] D. B. Bekker-Jensen, A. Martínez-Val, S. Steigerwald, P. Rüther, K. L. Fort, T. N. Arrey, A. Harder, A. Makarov, J. V. Olsen, *Mol. Cell. Proteomics* **2020**, *19*, 716.
[38] J. Cox, I. Matic, M. Hilger, N. Nagaraj, M. Selbach, J. V. Olsen, M. Mann, *Nat. Protoc.* **2009**, *4*, 698.
[39] A. D. Shah, R. J. A. Goode, C. Huang, D. R. Powell, R. B. Schittenhelm, *J. Proteome Res.* **2020**, *19*, 204.
[40] L. Väremo, J. Nielsen, I. Nookaew, *Nucleic Acids Res.* **2013**, *41*, 4378.
[41] X. Chen, X. Li, B. Ji, Y. Wang, O. P. Ishchuk, E. Vorontsov, D. Petranovic, V. Siewers, M. K. M. Engqvist, *Metab. Eng.* **2022**, *72*, 311.
[42] Y. Perez-Riverol, A. Csordas, J. Bai, M. Bernal-Llinares, S. Hewapathirana, D. J. Kundu, A. Inuganti, J. Griss, G. Mayer, M. Eisenacher, E. Pérez, J. Uszkoreit, J. Pfeuffer, T. Sachsenberg, Ş. Yılmaz, S. Tiwary, J. Cox, E. Audain, M. Walzer, A. F. Jarnuczak, T. Ternent, A. Brazma, J. A. Vizcaíno, *Nucleic Acids Res.* **2018**, *47*, D442.